SCIENTIFIC REPORTS

OPEN

SUBJECT AREAS:
BLOOD-BRAIN BARRIER
NANOBIOTECHNOLOGY

Received
15 November 2013

Accepted
14 March 2014

Published
15 April 2014

Correspondence and requests for materials should be addressed to P.C.S. (searson@jhu.edu)

# Brain microvascular endothelial cells resist elongation due to curvature and shear stress

Mao Ye[1,2], Henry M. Sanchez[2,3], Margot Hultz[2,3], Zhen Yang[4], Max Bogorad[2,3], Andrew D. Wong[2,3] & Peter C. Searson[1,2,3]

[1]Department of Physics and Astronomy, Johns Hopkins University, Baltimore, Maryland 21218, [2]Institute for Nanobiotechnology (INBT), Johns Hopkins University, Baltimore, Maryland 21218, [3]Department of Materials Science and Engineering, Johns Hopkins University, Baltimore, Maryland 21218 and, [4]Department of Electrical and Computer Engineering, Johns Hopkins University, Baltimore, Maryland 21218.

**The highly specialized endothelial cells in brain capillaries are a key component of the blood-brain barrier, forming a network of tight junctions that almost completely block paracellular transport. In contrast to vascular endothelial cells in other organs, we show that brain microvascular endothelial cells resist elongation in response to curvature and shear stress. Since the tight junction network is defined by endothelial cell morphology, these results suggest that there may be an evolutionary advantage to resisting elongation by minimizing the total length of cell-cell junctions per unit length of vessel.**

The diameter of blood vessels in humans ranges from about 8 μm in capillaries to more than 1 cm in large elastic arteries, a range of more than four orders of magnitude[1]. In larger vessels there are hundreds of cells around the perimeter, whereas in a capillary a single endothelial cell may wrap around to form a junction with itself as well as its upstream and downstream neighbors[2–6]. Since vessel diameters, and hence curvatures ($\kappa = 1/r$ where r is the vessel radius), span such a large range, we consider the question: does curvature play a role in dictating endothelial cell morphology (Figure 1a).

Curvature is a fundamental physical property that influences a wide range of everyday processes. For endothelial cells in vessels, if curvature is energetically unfavorable, then its effects can be minimized by elongating along the length of the vessel to avoid wrapping around in the radial direction. Conversely, if curvature is energetically favorable then cells may elongate in the radial direction to wrap around the vessel and contract in the axial direction (Figure S1 in *Supplementary Information*). How a cell responds to curvature and shear stress is important since junctional networks are defined by endothelial cell morphology. For example, for a fixed projected cell area and vessel diameter, elongation increases the number of cells around the perimeter and results in an increase in the total length of cell-cell junctions per unit length of vessel. Since tight junctions in brain capillaries are responsible for preventing paracellular transport, we hypothesize that cell morphology may play an important role in the structure and function of the blood-brain barrier.

Previous studies of the influence of curvature on cell behavior have focused on the motility of isolated cells in the context of tumor cell invasion[7–12]. Isolated fibroblasts seeded on small diameter glass rods (<200 μm) were shown to exhibit preferential elongation and alignment[7–9], and preferential migration along the cylinder axis, leading to the concept of contact guidance as a possible mechanism for tumor cell invasion[7]. These studies suggest that curvature may play a role in regulating the morphology and function of endothelial cells in confluent monolayers.

While the influence of curvature has been relatively unexplored, the role of shear stress on endothelial cell morphology and function has been more widely studied. Blood flow results in a frictional drag, or shear stress, on the vessel wall parallel to the endothelium in the direction of flow. These stresses play an important role in regulating endothelial cell morphology and function, and in mediating a wide range of signaling and transport processes between the vascular system and surrounding tissue[13–18]. Endothelial cells in blood vessels in sections away from branch points show elongation and axial alignment[19,20]. In cell culture, a physiological shear stress results in a transition from a cobblestone-like morphology to an elongated spindle-like morphology and alignment in the direction of flow[21–25], very similar to the morphology observed in large resected vessels.

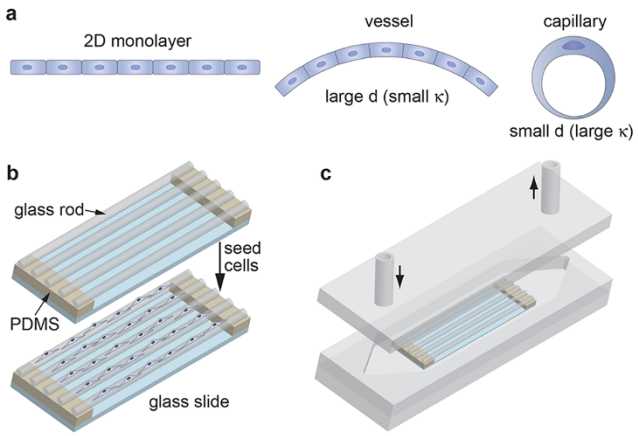


**Figure 1 | (a) Curvature ($\kappa = 1/r$) in confluent monolayers of endothelial cells.** In 2D monolayers the curvature is zero. In large diameter vessels the curvature is relatively small whereas in capillaries, cells may wrap around to form tight junctions with themselves, resulting in high curvature. (b) In the rod assay, cells are seeded on rods with different diameters and cell morphology determined from quantitative analysis of confocal microscope images. (c) Schematic illustration of the microfluidic device incorporating an array of glass rods seeded with confluent monolayers of endothelial cells.

To test the hypothesis that curvature and shear stress regulate endothelial cell morphology we developed the rod assay to mimic the cylindrical geometry of a blood vessel. While the rod assay is "inside out" in that the luminal sides of the cells are in contact with basement membrane on the rod, and the abluminal side is in contact with media, it is a convenient method to study the role of curvature on cell morphology over a wide range of diameters, from small capillaries to larger vessels. Using this assay we show quantitatively that brain microvascular endothelial cells, in contrast to endothelial cells in other organs, do not elongate in response to curvature and shear stress.

## Results

Human brain microvascular endothelial cells (HBMECs) were seeded onto glass rods with diameters from 10–500 μm, spanning the range from brain capillaries to larger vessels, and allowed to reach confluence. For comparison, experiments were also performed with HUVECs, widely used in cell culture studies of endothelial cells. Typical confocal microscope images of cells seeded onto rods with different diameters are shown in Figures 2a–f. To visualize the cell boundaries we stained for the tight junction protein ZO-1 in HBMECs and VE-cadherin in HUVECs. The junctional markers reveal the morphology of the cells on the surface of the rods. At the smallest rod diameters, the HBMECs wrap around to form junctions with themselves (see Figure 2c and 2i), whereas the HUVEC cells do not (see Figure 2f and 2l). Additional images, including cross-sections, are shown in Figure S2 in *Supplementary Information*.

The immunofluorescence images are transposed onto a 2D plane (Figure 2g–l) using custom software developed in our lab (see user manual in Supplementary Information). Image analysis software (e.g. ImageJ) is then used for quantitative analysis of cell morphology on the "unwrapped" images. Using this approach we can quantitatively determine parameters associated with cell morphology such as the projected cell area (A), perimeter (P), circularity ($C = 4\pi A/P^2$), inverse aspect ratio (IAR, length of short axis divided by length of long axis), and the orientation angle of the cell long axis with respect to the rod axis ($\theta$). We also used these unwrapped images for quantitative analysis of actin filament orientation using Fourier transformation.

**Elongation and alignment.** The dependence of morphological parameters on rod diameter for immortalized HBMECs and HUVECs is summarized in Figures 2m–p. Data for 2D monolayers are provided for comparison (Figure S3 in *Supplementary Information*) and additional data on cell area and perimeter are provided in Figure S4 in *Supplementary Information*. For HBMECs, the inverse aspect ratio (IAR), a measure of cell elongation, is only weakly dependent on curvature (Figure 2m). For rod diameters larger than 25 μm, the IAR is about 0.7, independent of diameter, whereas for rod diameters less than 25 μm, the IAR decreases slightly to about 0.65 at a diameter of about 10 μm. In contrast, the IAR for HUEVCs is strongly dependent on curvature, decreasing from about 0.6 at the largest diameter ($d > 400$ μm) to about 0.2 at the smallest rod diameter ($d \approx 10$ μm) (Figure 2m). Similar trends are observed for the cell circularity, a parameter commonly used in measuring cell morphology (Figure 2n). The small changes in IAR and circularity of HBMECs indicate that they are not sensitive to curvature and elongate only slightly as the rod diameter decreases below 25 μm. In contrast, HUVECs elongate along the rod axis with decreasing rod diameter instead of wrapping around the rod, thereby minimizing the effect of curvature (Figure S1 in *Supplementary Information*).

The average orientation angle of HBMECs is a measure of the axial alignment of cells (Figure 2o). On large diameter rods and in 2D monolayers, the average orientation angle is 45°, characteristic of a random distribution between 0–90° across all cells. The orientation remains random for rod diameters down to about 25 μm, further supporting the conclusion that the HBMECs are relatively insensitive to curvature. For rod diameters less than 25 μm, the average orientation angle decreases very rapidly to around 15° as the diameter approaches 10 μm. This decrease in orientation angle is a finite size effect due to the fact that the cell length is larger than the rod perimeter ($\pi d$), prohibiting large angles and hence shifting the distribution to smaller angles (Figure S5 in *Supplementary Information*). This effect is confirmed from analysis of the distribution of cell lengths and orientation angles (Figure S6 in *Supplementary Information*). In summary, HBMECs are slightly elongated (IAR = 0.7) and randomly oriented for all rod diameters and in 2D confluent monolayers.

In contrast, the average orientation angle of HUVECs decreases very quickly, reaching a value of less than 15° at a rod diameter of about 200 μm, and approaching 0° for the smallest diameter (11 μm). Even on the largest diameter rods, the curvature is sufficient to cause significant cell alignment. In summary, HUVECs are extremely sensitive to curvature, and begin to elongate and align even at the largest rod diameters. At the smallest diameters, the IAR decreases to about 0.2 corresponding to an elongation of five times, and the average orientation angle approaches zero corresponding to almost complete alignment.

The effect of curvature on endothelial cell morphology can be compared to the effect of shear stress. Analysis of endothelial cells in aortic vessels of dogs and rabbits reveals an IAR ≈ 0.2 (C ≈ 0.3) and an average orientation angle of 5–15°[19,26,27]. These values for IAR and orientation angle are similar to those reported here for HUVECs on rod diameters of about 10 μm suggesting that curvature has a similar effect to shear stress *in vivo*. In 2D cell culture, bovine aortic endothelial cells and HUVECs are characterized by IAR ≈ 0.7 (C ≈ 0.8) and $\theta \approx 45°$[21,22]. However, under a shear stress of 20–85 dynes $cm^{-2}$ for 24 h, the IAR decreases to about 0.25 (C ≈ 0.4) and $\theta$ to about 15°[21], further suggesting that curvature and physiological shear stress have a similar effect on cell morphology.

The differences in cell morphology between HBMECs and HUVECs are associated with differences in the actin cytoskeleton (Figure S2 in *Supplementary Information*). In HBMECs, actin stress fibers in the cell appear preferentially oriented perpendicular to the rod axis around the circumference (Figures S2b and S2d in

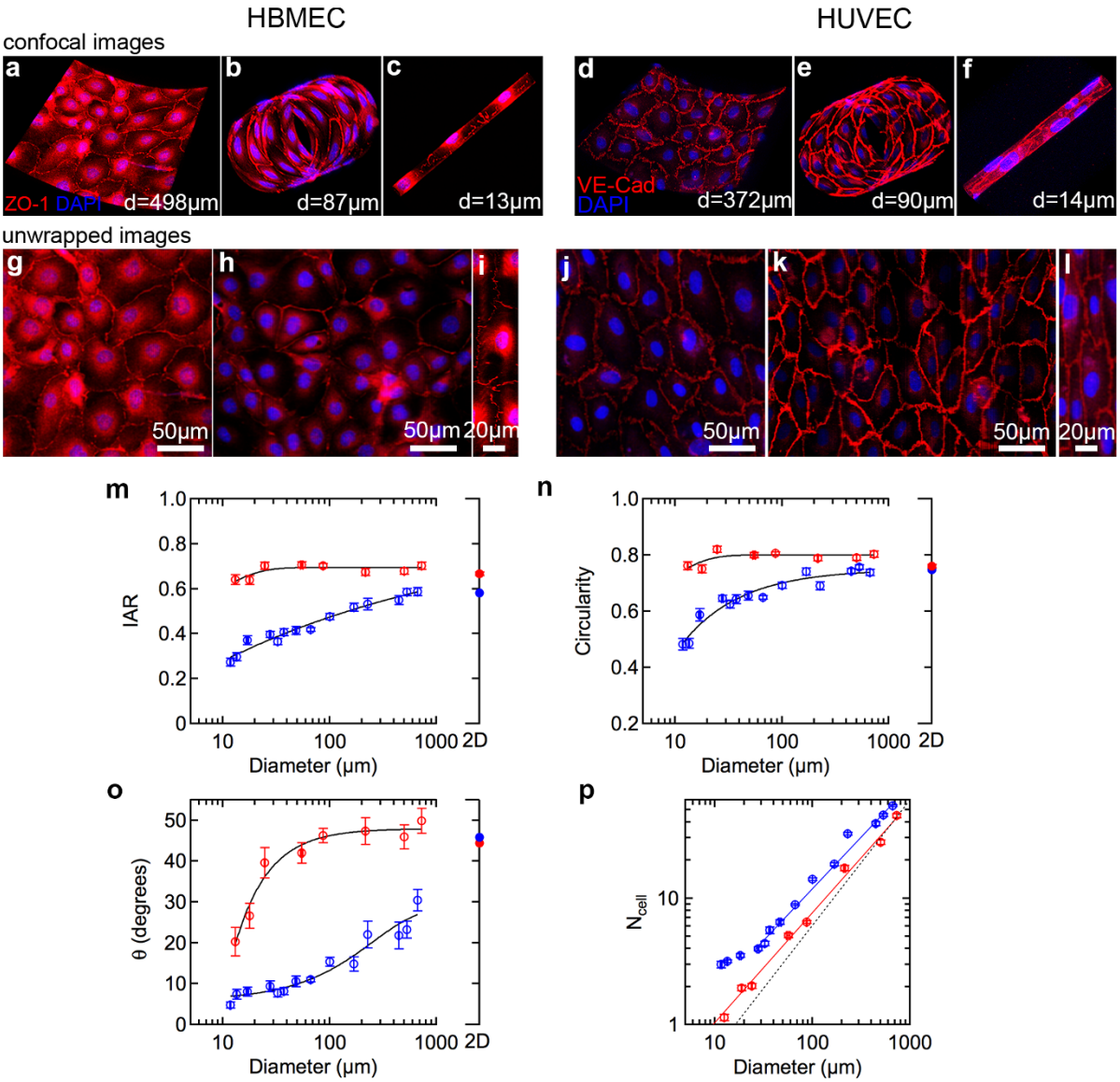


**Figure 2** | Confocal microscope images of confluent monolayers of (a–c) HBMECs and (d–f) HUVECs on rods with different diameter. HBMECs: (a) d = 498 μm, (b) d = 87 μm, (c) d = 13 μm. ZO-1 (red), DAPI (blue). HUVECs: (d) d = 372 μm, (e) d = 90 μm, (f) d = 14 μm. VE-Cadherin (red), DAPI (blue). Scaling in xy direction 0.44 μm/pixel, scaling in z direction 0.8 μm/pixel. (g–l) Unwrapped confocal microscope images of confluent monolayers of HBMECs and HUVECs on rods with different diameter. (m–o) Cell morphological parameters for confluent monolayers of HBMECs and HUVECs on rods with different diameters. Data for 2D confluent monolayers (labeled as 2D) are also shown for comparison. Inverse aspect ratio (IAR) is the length of the short axis divided by the length of the long axis, circularity, $C = 4\pi A/P^2$, and the orientation angle θ is the angle between the cell long axis and the rod axis. The total number of cells analyzed was 923 for HBMEC and 1306 for HUVEC. Error bars represent SE. (p) Average number of cells around the rod perimeter for HBMECs and HUVECs. The solid lines show fits to a power law where $N \propto d^{\alpha}$. For HBMECs $\alpha = 0.86$ and the x-axis intercept where N = 1 is at d = 9.8 μm. For HUVECs, $\alpha = 0.80$ and the x-axis intercept where N = 1 is at d = 4.4 μm. The dotted line shows $\alpha = 1.0$. Error bars represent standard error.

*Supplementary Information*). This is particularly striking for the smallest rod diameters (Figures S2f and S2h in *Supplementary Information*). In contrast, the stress fibers in HUVECs appear preferentially oriented in the axial direction (Figures S2k and S2m in *Supplementary Information*), and this is particularly evident at small rod diameters (Figures S2o and S2q in *Supplementary Information*).

**Scaling.** In brain capillaries, HBMECs wrap around the capillary perimeter to form tight junctions with themselves as well as their neighbors. To investigate how endothelial cells arrange themselves as the rod diameter decreases, we analyzed the number of cells around the perimeter of the rods (Figure 2p). For HBMECs, the number of cells around the perimeter of the rod decreases with decreasing radius, following a power law ($N \propto d^{\alpha}$) with an exponent $\alpha = 0.86$, down to the smallest diameter where cells wrap around the rod to form junctions with themselves and their neighbors, as observed in brain capillaries. The x-axis intercept at N = 1 (i.e. a single cell wrapping around to form a junction with itself) corresponds to a rod diameter of 9.8 μm, very close to typical human brain capillary dimensions. For a fixed IAR and projected cell area, the number of cells around the perimeter of a rod is expected to decrease linearly with diameter with an exponent $\alpha = 1.0$. The exponent of 0.86 is consistent with the small elongation.

The number of HUVEC cells around the perimeter also follows a power law down to about 30 μm in diameter with an exponent of

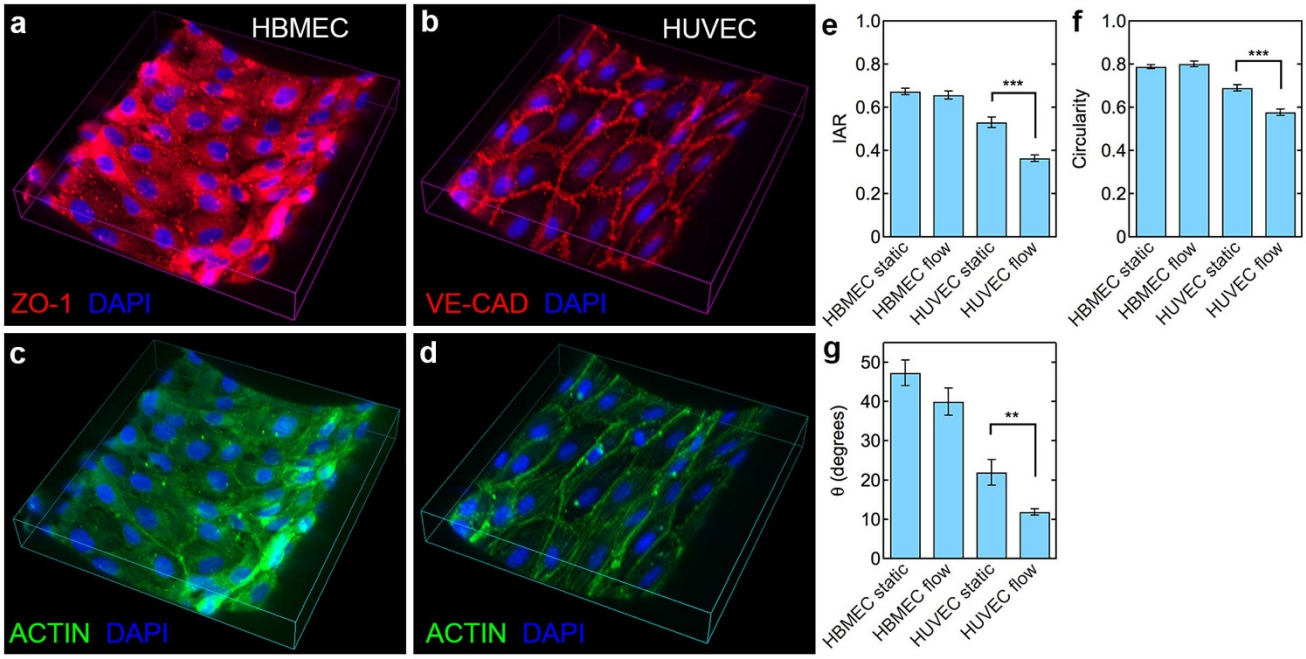


**Figure 3 | Influence of shear stress and curvature on cell morphology.** Cells were seeded on rods with average rod diameter of 217 ± 0 μm (HBMEC) and 228 ± 1 μm (HUVEC) and subjected to a shear stress of 50 dyne $cm^{-2}$ for 24 hours. (a), (c) HBMEC, (b), (d) HUVEC. (e) IAR, (f) circularity, and (g) average orientation angle (θ). HBMEC static (N = 72), HBMEC shear stress (N = 45), HUVEC static (N = 46), HUVEC shear stress (N = 92). *** $P < 0.001$, ** $P < 0.01$. For HUVEC: $P = 1.2 \times 10^{-7}$ (IAR), $P = 2.4 \times 10^{-7}$ (C), $P = 3.9 \times 10^{-3}$ (θ). Error bars represent SE.

0.80. The decrease in IAR (Figure 2m) and projected cell area both contribute to the smaller exponent compared to HBMECs. For rod diameters less than about 30 μm, the number of cells around the perimeter does not decrease below 3, indicating that there is a larger energy barrier for HUVECs to spread in regions of very high curvature compared to HBMECs (Figure S1 in *Supplementary Information*). Furthermore, the x-axis intercept at N = 1 corresponds to a rod diameter of 4.4 μm, below the typical human capillary diameter of around 8 μm, suggesting that HUVECS would not be able to wrap around and form junctions with themselves in capillaries, even without the deviation from power law behavior.

**Non-brain microvessels.** Assuming that HBMECs and HUVECs are representative of endothelial cells in brain microvessels and non-brain large vessels, respectively, then the cell morphology and distribution of actin stress fibers suggest that endothelial cells in brain microvessels may be programmed to respond to curvature differently than endothelial cells in larger vessels. To compare the behavior of endothelial cells in brain and non-brain microvessels, we studied the morphology of human dermal microvascular endothelial cells (HMVECs) in 2D and on glass rods with diameters around 20 and 200 μm (see Figure S7 and S8 in *Supplementary Information*). These results show that HMVECs behave similarly to HUVECs in all conditions, with morphological parameters (i.e. IAR, circularity, and orientation angle) significantly different from HBMECs in response to curvature ($P < 0.001$). This suggests it is the organ (brain or non-brain) rather than the vessel size that dictates the endothelial cell phenotype.

**Shear stress.** To assess the influence of curvature and shear stress on cell morphology, we subjected approximately 250 μm diameter rods with confluent monolayers of HBMECs and HUVECs to a shear stress of about 50 dyne $cm^{-2}$ for 24 hours (Figure 3). Analysis of cell morphology revealed no significant change in IAR, circularity, or alignment for HBMECs. In contrast, HUVEC cells showed a significant increase in elongation and alignment under shear stress compared to static conditions. However, these changes were smaller than induced by curvature, further highlighting the important role for curvature in regulating cell morphology. For example, the IAR of HUVECs on 228 μm rods decreased from 0.53 under static conditions to 0.36 under shear stress (Figure 3e). In contrast, the IAR decreased from 0.58 in 2D confluent monolayers to 0.27 on 12 μm diameter rods under static conditions (Figure 2m).

The distribution of actin stress fibers in the cells also shows significant differences between HBMECs and HUVECs. Quantitative analysis of actin filament orientation from the unwrapped confocal microscope images is shown in Figures S9 and S10 in *Supplementary Information*. In HBMECs, the stress fibers are oriented in all directions but with noticeably more fibers aligned perpendicular to the rod axis. In contrast, the stress fibers in HUVECs are predominantly aligned along the rod axis. In 2D experiments with bovine aortic endothelial cells and HUVECs, shear stress results in a reversible transition from a cobblestone morphology to a spindle morphology with the long axis aligned in the direction of flow. At the same time there is a reorganization in the actin cytoskeleton resulting in the formation of bundles of stress fibers aligned in the direction of flow[21,28]. The different alignment of stress fibers suggests that curvature influences cytoskeleton organization. This may be similar to the way that mechano-transduction of shear stress associated with blood flow plays a role in the regulation of physical, biochemical, and gene expression responses in arterial circulation[13,14,24].

## Discussion

There are 600 km of capillaries in brain that supply essential fuels and prevent entry of harmful chemicals, pathogens, and immune cells into the brain. The highly specialized endothelial cells that form brain capillaries are a key component of the blood-brain barrier (BBB) forming a network of tight junctions that almost completely block paracellular transport[3,4,29]. Spatially, the tight junction network that contributes to maintaining homeostasis in the brain is defined by the morphology of the endothelial cells that form the capillaries. Therefore, factors that affect cell morphology, such as blood flow and curvature, directly influence the tight junction network.

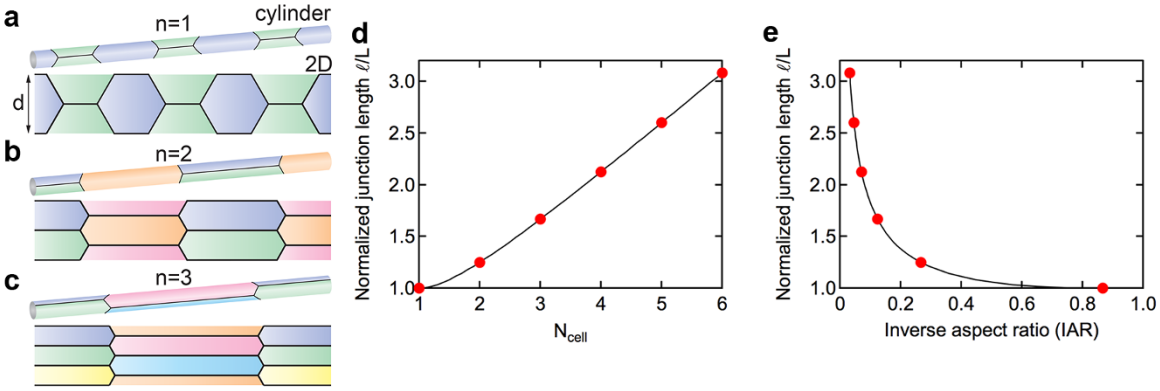


**Figure 4 | Relationship between endothelial cell morphology and tight junction length.** (a–c) Illustrations of junction networks for 1, 2, and 3 cells around the perimeter of a cylinder with fixed vessel diameter. The cell shape is assumed to be hexagonal (regular or irregular) with constant area and aligned in the axial direction. (d) Normalized junction length per unit length of cylinder versus number of cells around the perimeter. (e) Normalized junction length versus the inverse aspect ratio (assuming all cells are aligned in the axial direction). Note that the inverse aspect ratio (IAR) for a regular hexagon is 0.87.

To illustrate the relationship between cell morphology and the tight junction network, we consider a simple model (Figure 4) where cells of fixed area are tiled onto a cylinder of fixed vessel diameter. Cells are assumed to be hexagonal in shape and aligned in the axial direction. This model illustrates that the length of tight junctions per unit length of vessel decreases with decreasing elongation (IAR).

The paracellular flux of a solute (per unit length of capillary) into the brain is determined by the permeability (per unit length of tight junction) and the length of tight junctions (per unit length of capillary). Therefore to minimize brain penetration there is an advantage to minimizing the permeability and/or the length of tight junctions per unit length of capillary. In the brain, the permeability term is minimized by forming specialized tight junctions. To minimize the length of tight junctions (per unit length of capillary), brain microvascular endothelial cells should not elongate in response to the high curvature associated with small capillaries or shear stress associated with blood flow. The results from our rod assay suggest that brain microvascular endothelial cells are programmed to resist elongation in response to curvature and shear stress, and provide support for the hypothesis that this phenotype may have evolved to minimize the length of tight junctions per unit length of capillary and hence minimize paracellular transport into the brain.

## Methods

**Rod assay.** Glass rods 0.125 inches in diameter (Fisher Scientific, 11-380A) were pulled to a diameter in the range of 10–750 μm in a flame. The rods were cut into 2 cm lengths, selected for a particular diameter and uniformity under an optical microscope, and then mounted across two polydimethylsiloxane (PDMS) supports (Dow Corning, Sylgard 184) on a 22 mm × 22 mm glass slide (Fischer Scientific, 12542B). The rods were then immobilized with an additional drop of PDMS on top of the supports and cured at 80°C for about 15 minutes. Prior to seeding cells, the rod assemblies were oxygen plasma cleaned for 30 seconds, and incubated in 150 μg ml$^{-1}$ type I collagen (BD, 354236) solution in 0.02 M acetic acid (Fisher Scientific, A38-500) at room temperature for 1 to 2 hours, and then washed 3 times in PBS buffer (Corning Cellgro, 21-031-CV), followed by a final wash in cell culture medium.

**Seeding cells.** Human brain microvascular endothelial cells (HBMECs) were isolated from an adult brain and immortalized by transfection with SV40[30–32]. HBMEC cell culture medium was prepared by dissolving HEPES-modified M199 powder (Sigma Aldrich, M2520) in 1 liter distilled water and adding 10 vol% FBS (Life Technologies, 16140071), 1 vol% penicillin-streptomycin (Life Technologies, 15140122), and 2.2 g l$^{-1}$ sodium bicarbonate (Sigma Aldrich, S5761). Human umbilical vein endothelial cells (HUVECs, Lonza, CC-2517A) were suspended in the recommended cell culture medium (basal media with growth factors, Lonza, CC-3162). Human dermal microvascular endothelial cells (HMVECs, Life Technologies, C-011-5C) were cultured in medium prepared by dissolving 10 vol% FBS (Life Technologies, 16140071), 1 μg ml$^{-1}$ hydrocortisone (Sigma Aldrich, H0888), 2 U ml$^{-1}$ heparin (porcine intestinal mucosa, sodium salt, Sigma Aldrich, H3149), 25 μg ml$^{-1}$ endothelial cell growth supplement (Biomedical Technologies, BT-203), 0.2 mM L-ascorbic acid 2-phosphate (Sigma Aldrich, A8960), 1 vol% glutamine-penicillin-streptomycin (Life Technologies, 10378-016) in MCDB 131 (Caisson Labs, MBL02). All endothelial cells were routinely passaged at a 1 : 4 ratio, and were discarded after passage 5.

Approximately $10^6$ cells in 2 ml of medium were introduced into each dish containing a set of collagen-coated rods. The cell culture medium was changed every day by adding 2–3 ml of fresh medium into the petri dish, mixing it well, removing the same amount, and repeating at least 3 times. The cells generally began to spread on the rods after one day and if the coverage was about 60%, and reached confluence after 3–4 days. For control experiments in 2D, glass bottom petri dishes (BD, FD35PDL-100) were plasma treated for 30 seconds, coated with 150 μg ml$^{-1}$ type I collagen (BD, 354236) solution in 0.02 M acetic acid for 1–2 hours, and washed 3 times with PBS and once in cell culture medium prior to seeding with cells.

**Shear stress.** To study the effects of shear stress and curvature, a set of 200 μm rods was located parallel to the flow direction in a custom microfluidic device 40 mm long, 10 mm wide, and 2 mm high. The rods were typically 100 μm from the bottom of the channel. The device was placed in an incubator maintained at 37°C and 5% $CO_2$. Experiments were performed at a constant flow rate of 640 ml min$^{-1}$ using a peristaltic pump (Cole Parmer, WU-07523-80). The wall shear stress for a Newtonian fluid is given by $\tau = 6\,\mu Q/(wh^2)$, where μ is the viscosity (0.001 Pa s), Q is the flow rate, w is the channel width, and h is the channel height. From COMSOL simulations (see Figure S11 in *Supplementary Information*) we determined that the shear stress on the upper quadrant of the rods was 50 dyne cm$^{-2}$, decreasing to about 25 dyne cm$^{-2}$ at the sides. Quantitative analysis of morphology was performed for cells on the upper quadrant. After seeding cells on the rods and allowing them to reach confluence, the flow rate was set to about 40 ml min$^{-1}$ for 1 hour, and then gradually increased to 640 ml min$^{-1}$ over 6 hours, and then maintained at this value for 24 hours prior to removing the rods for analysis.

**Imaging.** Cells on collagen-coated rods were fixed and stained for ZO-1 (BD, 610967) or VE-cadherin (Life Technologies, 61-7300) and DAPI (Sigma Aldrich, D9542-1MG). Cell monolayers on rods were imaged using a confocal microscope (Zeiss LSM 510 META). Before imaging, the glass rods were removed from the assembly and placed on a 170 μm thick glass bottomed petri dish (World Precision Instruments, FD5040-100), and incubated in 2, 2′ – thioldiethanol (Sigma Aldrich, 166782). All images were obtained using a 40× oil-immersion objective (40 × 1.3 NA Plan Neofluar (oil)) in immersion oil (Zeiss, 444963-0000-000). Matching the refractive index of the rods is important to minimize distortion of the images. Z-stack images (512 × 512 pixel) were taken at 0.3–1.2 μm steps depending on the rod diameter.

**Image analysis.** For quantitative analysis of cell morphology the cylindrical immunofluorescence images of the cell monolayers were converted to a 2D plane using UNWRAP a custom application developed in our lab (see user manual in *Supplementary Information*). Morphological analysis was performed on the unwrapped 2D images using ImageJ (National Institute of Health, Bethesda, MD). After identification of the cell-cell boundaries, we determined projected cell area (μm$^2$), perimeter (μm), inverse aspect ratio (IAR) (length of short axis/length of long axis), and the orientation angle (θ), i.e. the angle between the cell long axis and the rod axis (0 to 90 degrees). The number of cells around the perimeter of the cylinder was determined by selecting a line perpendicular to the rod direction and counting the number of cells on the line. The line was then moved along the image in the direction of the rod axis until there were no previously counted cells along the line. For a given unwrapped image corresponding to a rod segment, we can usually extract about 3–4 measurements from each image. For HBMECs we made 14 – 62 measurements for each rod diameter (total = 303) and for HUVECs we made 18 – 117 measurements (total = 531).

The distribution of actin stress fibers was analyzed by performing 2D FFTs on the images. FFTs were performed using the FFT2 routine in MATLAB. The resulting intensity distributions in the frequency domain were converted to radial intensity distributions at 10° increments. For images on larger rods and 2D images were cropped to be 141 × 141 μm the resolution fixed at 0.44 μm per pixel. For images on smaller rods, images were cropped to be 93 × 93 μm with the resolution fixed at 0.44 μm per pixel.

Welch two sample t-tests were performed in MATLAB. Significant levels were determined between samples examined and were set at * $P < 0.05$, ** $P < 0.01$, and *** $P < 0.001$.


1. Aird, W. C. Spatial and temporal dynamics of the endothelium. *J. Thromb. Haemost.* **3**, 1392 (2005).
2. Abbott, N. J., Ronnback, L. & Hansson, E. Astrocyte-endothelial interactions at the blood-brain barrier. *Nat. Rev. Neurosci.* **7**, 41 (2006).
3. Daneman, R. The blood-brain barrier in health and disease. *Ann. Neurol.* **72**, 648 (2012).
4. Wong, A. D. *et al.* The blood-brain barrier: an engineering perspective. *Front. Neuroeng.* **6**, 7 (2013).
5. Reese, T. S. & Karnovsky, M. J. Fine structural localization of a blood-brain barrier to exogenous peroxidase. *J. Cell Biol.* **34**, 207 (1967).
6. Brightman, M. W. Morphology of Blood-Brain Interfaces. *Exp. Eye Res.* **25**, 1 (1977).
7. Curtis, A. S. G. & Varde, M. Control of cell behavior: topological factors. *J. Natl. Cancer Inst.* **33**, 15 (1964).
8. Dunn, G. A. & Heath, J. P. A new hypothesis of contact guidance in tissue cells. *Exp. Cell Res.* **101**, 1 (1976).
9. Fisher, P. E. & Tickle, C. Differences in alignment of normal and transformed cells on glass fibres. *Exp. Cell Res.* **131**, 407 (1981).
10. Rovensky, Y. & Samoilov, V. I. Morphogenetic response of cultured normal and transformed fibroblasts, and epitheliocytes, to a cylindrical substratum surface. Possible role for the actin filament bundle pattern. *J. Cell Sci.* **107**, 1255 (1994).
11. Svitkina, T. M., Rovensky, Y. A., Bershadsky, A. D. & Vasiliev, J. M. Transverse pattern of microfilament bundles induced in epitheliocytes by cylindrical substrata. *J. Cell Sci.* **108**, 735 (1995).
12. Levina, E. M., Domnina, L. V., Rovensky, Y. A. & Vasiliev, J. M. Cylindrical substratum induces different patterns of actin microfilament bundles in nontransformed and in RAS-transformed epitheliocytes. *Exp. Cell Res.* **229**, 159 (1996).
13. Hahn, C. & Schwartz, M. A. Mechanotransduction in vascular physiology and atherogenesis. *Nat. Rev. Mol. Cell Biol.* **10**, 53 (2009).
14. Chien, S. Mechanotransduction and endothelial cell homeostasis: the wisdom of the cell. *Am. J. Physiol. Heart Circ. Physiol.* **292**, H1209 (2007).
15. Johnson, B. D., Mather, K. J. & Wallace, J. P. Mechanotransduction of shear in the endothelium: basic studies and clinical implications. *Vasc. Med.* **16**, 365 (2011).
16. Conway, D. & Schwartz, M. A. Lessons from the endothelial junctional mechanosensory complex. *F1000 Biol. Rep.* **4**, 1 (2012).
17. Aird, W. C. Phenotypic heterogeneity of the endothelium: II. Representative vascular beds. *Circ. Res.* **100**, 174 (2007).
18. Aird, W. C. Phenotypic heterogeneity of the endothelium: I. Structure, function, and mechanisms. *Circ. Res.* **100**, 158 (2007).
19. Nerem, R. M., Levesque, M. J. & Cornhill, J. F. Vascular endothelial morphology as an indicator of the pattern of blood-flow. *J. Biomech. Eng. Trans. ASME* **103**, 172 (1981).
20. Reidy, M. A. & Langille, B. L. The effect of local blood flow patterns on endothelial cell morphology. *Exp. Mol. Pathol.* **32**, 276 (1980).
21. Malek, A. M. & Izumo, S. Mechanism of endothelial cell shape change and cytoskeletal remodeling in response to fluid shear stress. *J. Cell Sci.* **109**, 713 (1996).
22. Levesque, M. J. & Nerem, R. M. The elongation and orientation of cultured endothelial-cells in response to shear-stress. *J. Biomech. Eng. Trans. ASME* **107**, 341 (1985).
23. Eskin, S. G., Ives, C. L., Mcintire, L. V. & Navarro, L. T. Response of cultured endothelial-cells to steady flow. *Microvasc. Res.* **28**, 87 (1984).
24. Davies, P. F. Flow-Mediated Endothelial Mechanotransduction. *Physiol. Rev.* **75**, 519 (1995).
25. Simmers, M. B., Pryor, A. W. & Blackman, B. R. Arterial shear stress regulates endothelial cell-directed migration, polarity, and morphology in confluent monolayers. *Am. J. Physiol. Heart Circ. Physiol.* **293**, H1937 (2007).
26. Levesque, M. J., Liepsch, D., Moravec, S. & Nerem, R. M. Correlation of endothelial-cell shape and wall shear-stress in a stenosed dog aorta. *Arteriosclerosis* **6**, 220 (1986).
27. Silkworth, J. B. & Stehbens, W. E. Shape of endothelial cells in en-face preparations of rabbit blood-vessels. *Angiology* **26**, 474 (1975).
28. Franke, R. P. *et al.* Induction of human vascular endothelial stress fibres by fluid shear stress. *Nature* **307**, 648 (1984).
29. Abbott, N. J., Patabendige, A. A., Dolman, D. E., Yusof, S. R. & Begley, D. J. Structure and function of the blood-brain barrier. *Neurobiol. Dis.* **37**, 13 (2010).
30. Nizet, V. *et al.* Invasion of brain microvascular endothelial cells by group B streptococci. *Infect. Immun.* **65**, 5074 (1997).
31. Stins, M. F., Prasadarao, N. V., Zhou, J., Arditi, M. & Kim, K. S. Bovine brain microvascular endothelial cells transfected with SV40-large T antigen: development of an immortalized cell line to study pathophysiology of CNS disease. *In Vitro Cell. Dev. Biol. Anim.* **33**, 243 (1997).
32. Eigenmann, D. E. *et al.* Comparative study of four immortalized human brain capillary endothelial cell lines, hCMEC/D3, hBMEC, TY10, and BB19, and optimization of culture conditions, for an in vitro blood-brain barrier model for drug permeability studies. *Fluids Barriers CNS* **10**, 33 (2013).


## Acknowledgments

MY acknowledges Michael McCaffery and Erin Pryce for training in confocal microscopy at the Integrated Imaging Center (JHU).

## Author contributions

M.Y., A.D.W. and P.C.S. designed the experiments. M.Y., H.M.S., M.H. and M.B. performed the experiments. M.Y. and Z.Y. developed the UNWRAP application, M.Y. and P.C.S. analyzed the data, M.Y. and P.C.S. wrote the paper.

## Additional information

**Supplementary information** accompanies this paper at http://www.nature.com/scientificreports

**Competing financial interests:** The authors declare no competing financial interests.

**How to cite this article:** Ye, M. *et al.* Brain microvascular endothelial cells resist elongation due to curvature and shear stress. *Sci. Rep.* **4**, 4681; DOI:10.1038/srep04681 (2014).